2022 19th International Conference on Electrical Engineering, Computing Science and Automatic Control (CCE).
Mexico City, Mexico. November 9-11, 2022

Electrostatic Model for Semiconductor Radial Nanowire Heterojunctions

C. Joven-Rodríguez
Facultad de Ciencias Exactas y Naturales
Universidad Nacional de Colombia
Manizales, Colombia
cdjovenr@unal.edu.co

A. Morales-Acevedo
Sección de Eletrónica y Estado Solido
Centro de Investigación y de Estudios Avanzados del IPN
Ciudad de México, México
amorales@solar.cinvestav.mx

R. Bernal-Correa
Instituto de Estudios de la Orinoquia
Universidad Nacional de Colombia
Arauca, Colombia
rabernalco@unal.edu.co

***Abstract*— Radial nanowire semiconductor devices have become a practical possibility in recent years. Hence, high-efficiency solar cells based on radial nanowire heterojunctions can now be realized. In this study, an electrostatic model for radial nanowire heterojunctions was developed by solving Poisson´s equation in cylindrical coordinates. In contrast to planar one-dimensional homo and heterojunctions, in this case, transcendental equations must be solved numerically to determine the radial space-charge dimensions. The electric field and potential distribution in the radial heterojunction are also obtained and graphed for different polarization voltages. As examples, InP/Si heterojunction and InP homojunction nanowire structures are electrostatically studied. This work is intended to be the basis for developing a more complete model for radial nanowire heterojunction solar cells under sunlight.**

Keywords*— nanowire solar cells, heterojunctions, electrostatic models.

I. INTRODUCTION

Photovoltaic devices or solar cells have become an essential tool for harnessing solar energy, which is considered almost inexhaustible [1-3]. Currently, the scientific community is focusing its efforts on the study of new materials, the design of different architectures, and the implementation of new production technologies [4, 5], with the purpose of achieving higher performances and reducing the production costs of solar cells, allowing them to compete with other renewable and non-renewable energies [6].

Among the different generations of solar cells, the tandem multi-junction cells, the perovskite and the nanowire solar cells stand out [7-10] in the photovoltaic field. The latter are the most innovative since their design is significantly different from the others (flat solar cells). A higher carrier collection efficiency can be expected from nanowire solar cells since the charge is transported radially between the core and the surrounding shell coating [11] in a perpendicular direction to the sunlight propagation and absorption. In addition, light absorption in a nanowire can be higher than in a planar solar cell due to reduced light reflection on the top surface of the nanowire and better light capture [12]. Although there are recent advances that report high efficiencies of 15 to 17% [13-15], such devices are yet to be further explored.

It is significant to mention that the internal structure and distribution of semiconductors in nanowires change drastically for radial and axial configurations. In the case of radial nanowire cells, they have an architecture formed by a p or n-type core, and a shell coating of the opposite type (n or p) [16]. In the axial nanowire cells, the semiconductor distribution is on the central axis of the nanowire and is characterized by starting with the p or n-type material and the opposite material on it [17]. The radial architecture should be more efficient by the reasons explained above and therefore in this paper, this kind of devices will be studied.

The use of computational tools and simulations have allowed the prediction of physical parameters in solar cells, so much research has been reported [18, 19]. For radial nanowire solar cells, some reports include optical, electrostatic, and electrical models [20-23]. However, it is still necessary to propose additional models that adjust to the different designs in which a variety of materials and configurations can be included (arrangement of p- and n-type semiconductors in the core and coating).

In this work, we report a semi-analytical electrostatic model for the radial nanowire cells formed by core-shell hetero-junctions. Furthermore, in order to show the application of the model, examples for both heterojunction and homo-junction radial nanowire solar cells (Si/InP and InP/InP) are shown. Finally, we conclude that calculations based on this kind of model is a very important step to predict the performance of radial hetero-junction devices, considered a promising alternative for developing solar cells.

II. DEVICE DETAILS

For the case of nanowire heterojunctions with radial geometry, we assume a configuration consisting of two semiconductor regions: the core and the shell. Thus, it is possible to model P-N or N-P semiconductor radial heterojunctions. Figure 1 shows a complete view of the nanowire device, where we can appreciate the radius of the core (R_1) and the total radius of the device (R_2). L is the nanowire length; for a solar cell it must be of the order of the absorption length for the absorber material.

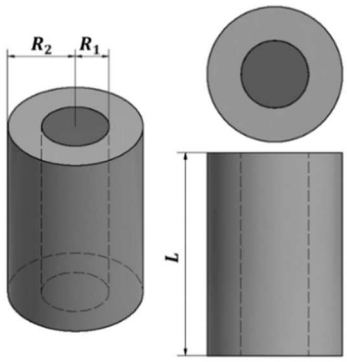

Fig. 1. Schematics of the full nanowire heterojunction device.

In Figure 2, the different device regions for a P-N heterojunction can be appreciated, formed by a P-type core semiconductor (R_1) and an N-type shell semiconductor (R_2-

978-1-6654-5508-4/22/$31.00 ©2022 IEEE

R_1). The space charge region extends along the P and N materials (being w_P and w_N, the respective space-charge region thicknesses), as indicated.

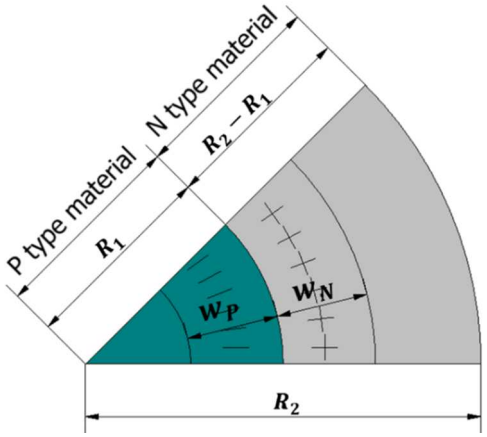

Fig. 2. Schematics of the P-N radial nanowire heterojunction dimensions.

III. MODEL DETAILS

Uniform n-type and p-type semiconductors will be assumed. Then, in a similar manner to a planar one-dimensional heterojunction, Poisson´s equation for the potential Φ must be solved:

$$\nabla^2\Phi = -\frac{\rho}{\epsilon} \qquad (1)$$

where ε is the dielectric constant of the material and ρ is the charge density.

Writing down the Laplacian operator in cylindrical coordinates and considering the length along the z dimension, the following equation in radial terms r, can be obtained:

$$\frac{1}{r}\frac{d}{dr}\left(r\frac{d\Phi}{dr}\right) = -\frac{\rho}{\epsilon} \qquad (2)$$

The general solutions for electric field E(r) and potential Φ(r) are below [22]:

$$E(r) = \frac{r\rho}{2\epsilon} - \frac{c_1}{r} \qquad (3)$$

$$\Phi(r) = -\frac{\rho r^2}{4\epsilon} + c_1 \ln r + c_2 \qquad (4)$$

where c_1 and c_2 are integration constants that can be found by applying the appropriate boundary conditions.

A. P-N heterojunctions

- *Core P*

The different regions are those shown in Figure 2, where R_1 is the P material radius and w_P is the space-charge region thickness in the P material, i.e., the region where ionized negative charges (with density N_A) within R_1.

The quasi-neutral zone in the core is bounded by $0 < r < R_1 - w_P$:

$$\begin{cases} E(R_1 - w_p) = 0 \\ \Phi(R_1 - w_p) = 0 \end{cases} \qquad (5)$$

With these boundary conditions, we get c_1 and c_2 for writing the full functions of the electric field and potential in the space-charge zone:

$$E(r) = -\frac{qN_A}{2\epsilon_1}\left(r - \frac{(R_1 - w_P)^2}{r}\right) \qquad (6)$$

$$\Phi(r) = \frac{qN_A}{4\epsilon_1}\left(r^2 - (R_1 - w_P)^2 - 2(R_1 - w_P)^2 \ln\left(\frac{r}{R_1 - w_P}\right)\right) \qquad (7)$$

where N_A is the acceptor concentration in the core material, ϵ_1 is the dielectric constant of the P-type material, and q is the electron´s charge magnitude.

- *Shell N*

The shell extends from R_1 to R_2. R_2 is the complete radius of the device, and w_N is the space-charge region in the shell. In the quasi-neutral region bounded by $R_1 + w_N < r < R_2$ there is no presence of electric field, but the potential reaches the built-in potential Φ_0 and remains constant in this region (without any applied voltage). Based on fig. 3, we can calculate the built-in potential using the following expression [24]:

$$\Phi_0 = \frac{kT}{q} ln\left(\frac{N_A N_D}{n_{iN} n_{iP}}\right) + \frac{1}{q}(\chi_N - \chi_P) + \left(\frac{E_{GN} - E_{GP}}{2q}\right) + \frac{kT}{q} ln\left(\frac{N_{VP} N_{CN}}{N_{VN} N_{CP}}\right) \qquad (8)$$

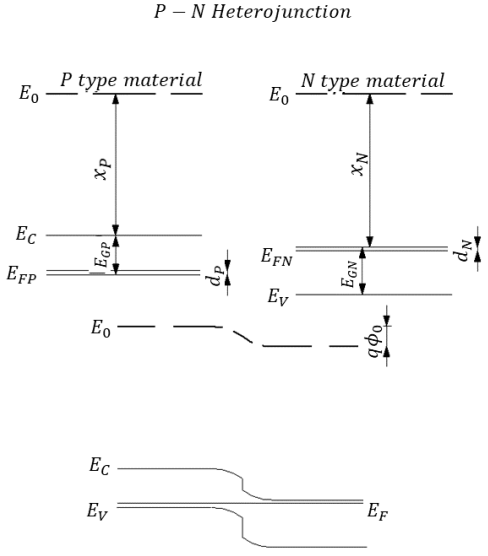

Fig. 3. General band diagram for a P-N heterojunctions.

where k is the Boltzmann constant, χ_P and χ_N are the electron affinities, E_{GP} and E_{GN} are the bandgaps, n_{iP} and n_{iN} are the minority carrier densities, N_{VP} and N_{VN} are the effective densities of states in the valence bands and N_{CP}, N_{CN} are the effective densities of states in the conduction bands for the P and N materials, respectively. For this region:

$$\begin{cases} E(R_1 + w_N) = 0 \\ \Phi(R_1 + w_N) = \Phi_0 \end{cases} \qquad (9)$$

The electric field and the potential in the space-charge region within the N-type shell can be determined as

$$E(r) = \frac{qN_D}{2\epsilon_2}\left(r - \frac{(R_1+w_N)^2}{r}\right) \qquad (10)$$

$$\Phi(r) = \Phi_0 - \frac{qN_D}{4\epsilon_2}\left(r^2 - (R_1+w_P)^2 - 2(R_1+w_P)^2 \ln\left(\frac{r}{R_1+w_P}\right)\right) \qquad (11)$$

where N_D is the donor concentration in the N-type shell material.

- *Electric displacement and potential continuity*

After checking the potential continuity at $r = R_1$, using the charge neutrality condition, and working the expressions for a given applied forward voltage V, the following transcendental equations for w_P and w_N can be obtained:

$$w_P = R_1 - \sqrt{\frac{\frac{4(\Phi_0-V)}{q} - \left[\frac{R_1^2(N_D+N_A)}{\epsilon_2}\right]\ln\left[\frac{N_A\left(R_1^2-(R_1-w_P)^2\right)}{N_D R_1^2}+1\right] - \frac{N_A R_1^2(\epsilon_2-\epsilon_1)}{\epsilon_2\epsilon_1}}{\frac{N_A}{\epsilon_1\epsilon_2}\left[(\epsilon_1-\epsilon_2) - \epsilon_2\ln\left[\frac{R_1^2}{(R_1-w_P)^2}\right] - \epsilon_1\ln\left[\frac{N_A\left(R_1^2-(R_1-w_P)^2\right)}{N_D R_1^2}+1\right]\right]}} \qquad (12)$$

$$w_N = \sqrt{\frac{\frac{4(\Phi_0-V)}{q} - \left[\frac{R_1^2(N_D+N_A)}{\epsilon_1}\right]\ln\left[\frac{N_D\left(R_1^2-(R_1+w_N)^2\right)}{N_A R_1^2}+1\right] - \frac{N_D R_1^2(\epsilon_1-\epsilon_2)}{\epsilon_2\epsilon_1}}{\frac{N_D}{\epsilon_1\epsilon_2}\left[(\epsilon_2-\epsilon_1) - \epsilon_1\ln\left[\frac{R_1^2}{(R_1+w_N)^2}\right] - \epsilon_2\ln\left[\frac{N_D\left(R_1^2-(R_1+w_N)^2\right)}{N_A R_1^2}+1\right]\right]}} - R_1 \qquad (13)$$

Similar expressions can be written straightforwardly for N-P radial heterojunctions where the core is N-type and the shell is P-type.

IV. RESULTS

To obtain results based on the above equations, a Python program was developed using the Newton-Raphson method to solve the transcendental equations (12) and (13). Once w_P and w_N are known, the electric field and the potential distributions can be calculated, using equations (6) to (11).

As an application of the above procedure, calculations were made for both radial nanowire heterojunctions and homojunctions. For the heterojunction case, a Si-P(core)/InP-N(shell) heterojunction was studied. On the other hand, for a homojunction example, an InP-P(core)/InP-N(shell) junction was used. The constants shown in tables 1 and 2 were used as reported by [25, 26].

TABLE I. Si CONSTANTS USED IN THE SIMULATION.

Constant	Value	Units
Effective density of states in conduction band (N_c)	$3.2 * 10^{25}$	$\left[\frac{1}{m^3}\right]$
Effective density of states in valence band (N_V)	$1.8 * 10^{25}$	$\left[\frac{1}{m^3}\right]$
Donor density (N_D)	$1 * 10^{23}$	$\left[\frac{1}{m^3}\right]$
Acceptor density (N_A)	$1 * 10^{23}$	$\left[\frac{1}{m^3}\right]$
Band gap (E_G)	1.11	eV
Electronic affinity (χ)	4.05	eV
Dielectric constant (ϵ)	$1.03 * 10^{-11}$	$\left[\frac{C^2}{Nm^2}\right]$

For the example simulation, the core and the shell radius were set to $R_1 = 50\,nm$ and $R_2 = 100\,nm$ for both the heterojunction and homojunction cases. Finally, the core radius variation effect upon the space charge region thickness w_P and w_N was studied, as explained below.

TABLE II. InP CONSTANTS USED IN THE SIMULATION

Constant	Value	Units
Effective density of states in conduction band (N_c)	$5.7 * 10^{23}$	$\left[\frac{1}{m^3}\right]$
Effective density of states in valence band (N_V)	$1.1 * 10^{25}$	$\left[\frac{1}{m^3}\right]$
Donor density (N_D)	$1 * 10^{23}$	$\left[\frac{1}{m^3}\right]$
Acceptor density (N_A)	Equal to N_D for the homojunction case	$\left[\frac{1}{m^3}\right]$
Band gap (E_G)	1.34	eV
Electronic affinity (χ)	4.38	eV
Dielectric constant (ϵ)	$4.78 * 10^{-11}$	$\left[\frac{C^2}{Nm^2}\right]$

A. Heterojuncions

For the heterojunction case, silicon is assumed to be the core material since it is experimentally easier to manufacture the nanowire device when InP is grown over the silicon, as is mentioned by [10]. Figure 4 shows the band diagram and the band discontinuity for the P-N heterojunction. The built-in potential is given in the diagram (1.4 V) for the simple case in which $N_A = N_D$.

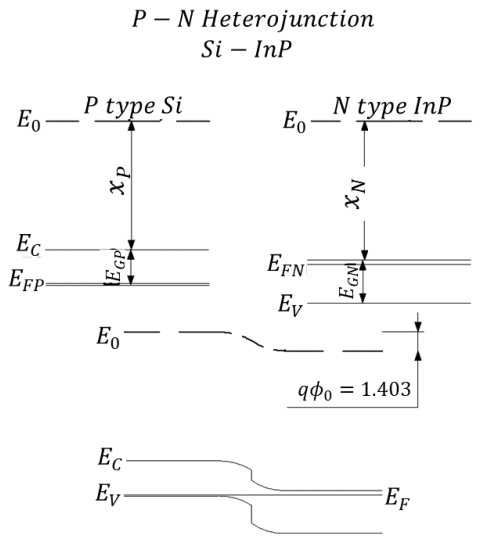

Fig. 4. Band diagram of the P-N Si/InP device.

Solving the expressions (12)-(13) by a Newton-Raphson method, the space-charge region thickness behavior as a function of the applied forward voltage is obtained (see Figure 5). The vertical dotted line corresponds to the forward critical voltage (Vc = 1.226 V) below which the core is completely depleted. For smaller applied voltages (V < Vc), the whole space-charge region thickness remains constant due to the charge neutrality restriction.

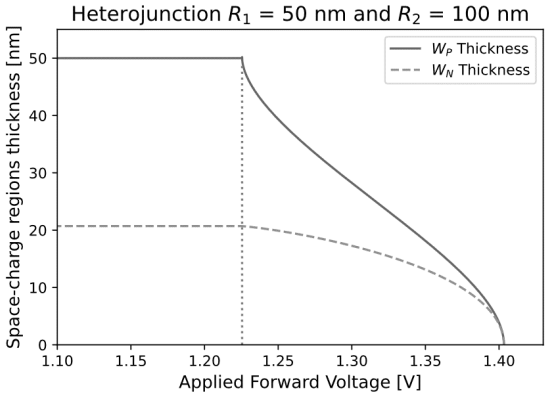

Fig. 5. Space charge thickness w_N and w_P for the Si(P)/InP(N) nanowire heterojunction diode.

Figure 6 (a) shows the electric field distribution across the radial direction for the P-N heterojunction. Notice the discontinuity at r = R_1 due to the different dielectric constants for each region (electric displacement should be continuous). Figure 6 (b) shows a top view of the electric field E for the critical applied voltage (Vc) above which the space charge region begins to shrink causing a reduction of the electric field magnitude.

Figure 7 (a) illustrates the electric potential for the heterojunction as a function of the radial distance from the device center for different voltages. Fig. 7 (b) help us seeing the potential distribution at the critical applied voltage Vc mentioned above.

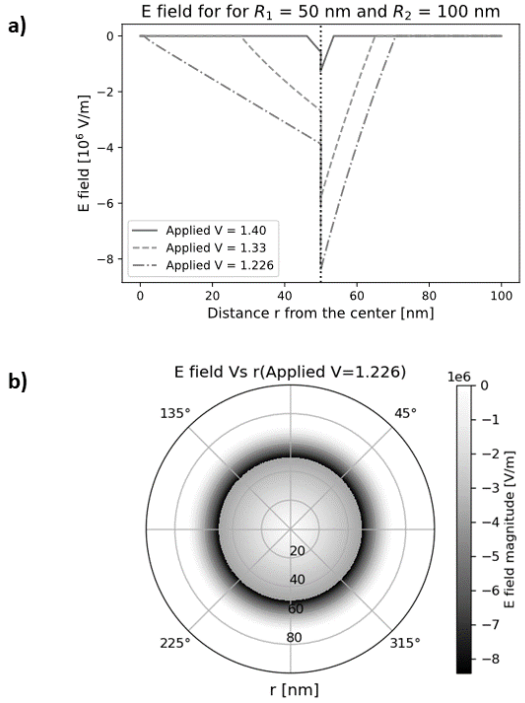

Fig. 6. a) Electric field in radial terms for the P-N Heterojunction b) Top view of E in the P-N Heterojunction.

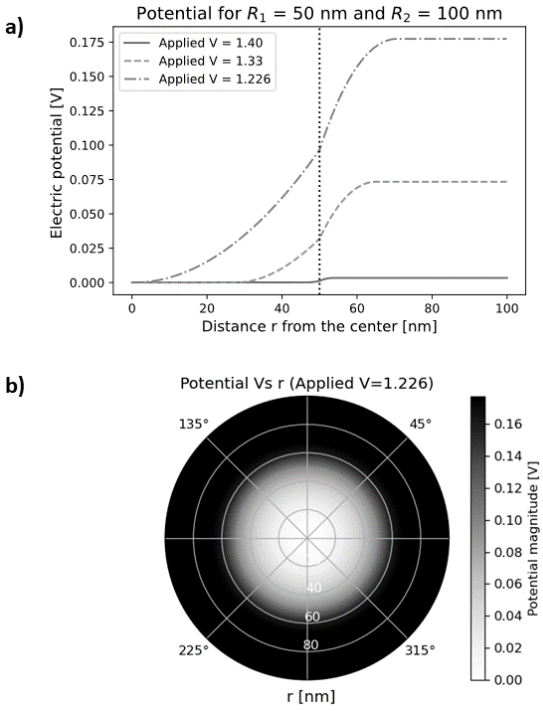

Fig. 7. a) Electric potential in radial terms for the P-N Heterojunction. b) Top view of the potential in the P-N Heterojunction.

B. Heterojunction core radius variation effect

It is expected that as the core radius is changed (keeping the total nanowire diameter constant) the critical voltage Vc will also change since this voltage is related to the total charge in this region. Then, for this purpose R_1=25, 50 and 75 nm were selected with constant R_2 = 100 nm, and the results are shown in Figure 8. In accordance with our expectation, the critical voltage Vc is changed from 1.23 V to 1.36 V when the core radius is changed from 50 nm down to 25 nm. In other words, the critical voltage Vc, below which the core is fully

depleted, is increased as the core radius is smaller. On the other hand, when R_1 = 75 nm the shell becomes fully depleted at the critical voltage around 1.19 V because, in this case, there is a smaller dimension available for W_N (R_2 - R_1 = 25 nm,) and a larger one for W_P.

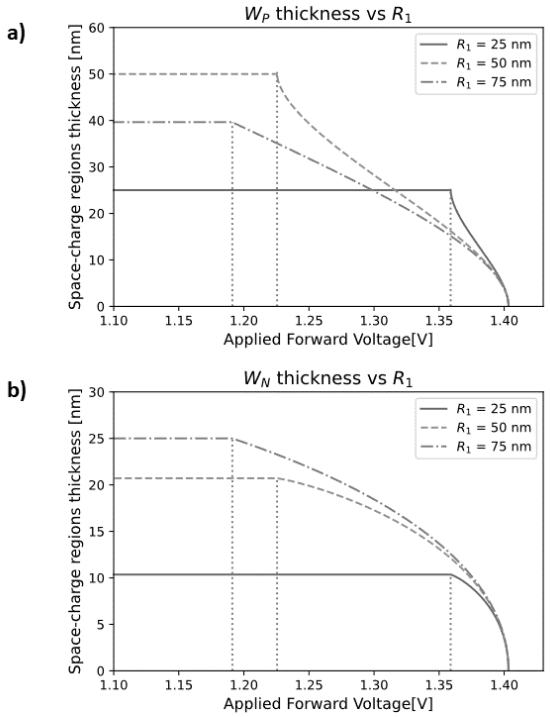

Fig. 8. a) w_P thickness as a function of the core radius. b) w_N thickness behavior as a function of the core radius, for three different R_1 values with a fixed R_2.

The kind of calculation explained above is important to determine the space charge region extension in solar cells because the photo-carrier collection probability will be dominated by carrier drift in the high electric field within the space charge region. We must take in account the transport in both the core and the shell regions, for an optimal design of the cell to achieve the highest total photo-current density and the minimum dark current density. Having a tool like the one developed here would help for achieving this purpose.

C. Homojunction

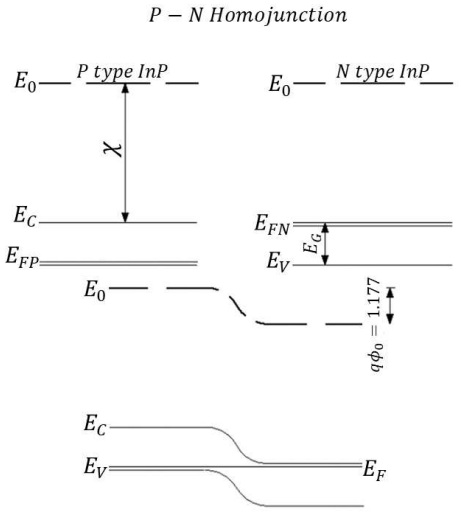

Fig. 9. InP homojunction band diagram.

Using the same expressions developed in general for heterojunction devices, nanowire homojunctions can also be studied. A radial nanowire InP homojunction was simulated in a P-N disposition, in the symmetric case where $N_A = N_D$. The InP homojunction band diagram, for the parameters given in table 2, is shown in Figure 9. The calculated built-in potential (1.177 V) is given in this diagram.

The result for the space-charge thickness as a function of the applied voltage is shown in fig. 10. In this case, the critical forward voltage Vc is 0.887 V. Below this voltage the P region is fully depleted, so that the space charge region thickness in the N-type shell is kept constant (due to the charge neutrality condition). For voltages above Vc both space charge regions thicknesses are reduced to zero when the applied voltage reaches the built-in potential. Figure 11 and Figure 12 show the electric field and the potential distributions, respectively.

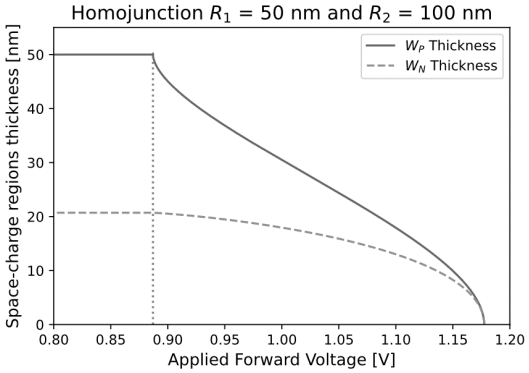

Fig. 10. Space charge thickness w_N and w_P for the symmetric InP P-N homojunction.

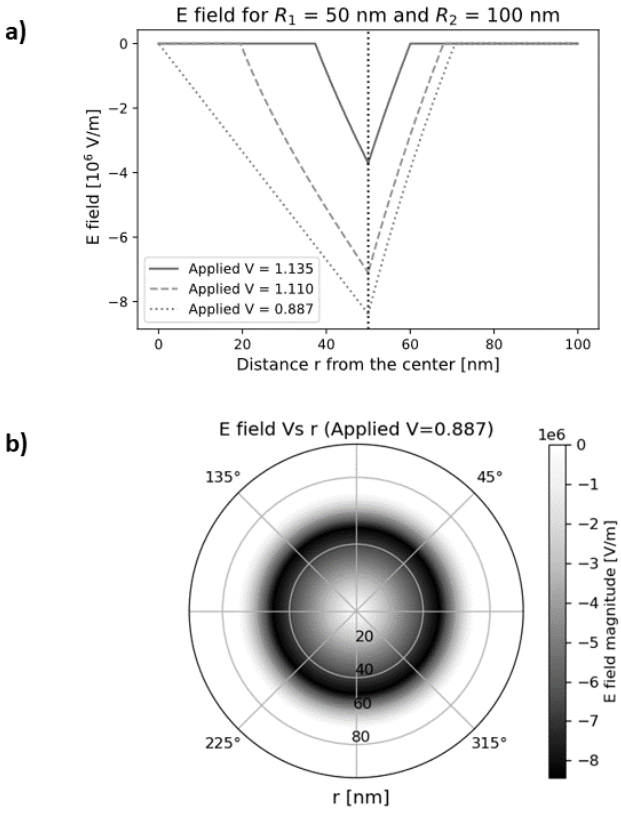

Fig. 11. a) Electric field in radial terms for the InP P-N homojunction. b) Top view of E in the InP P-N homojunction.

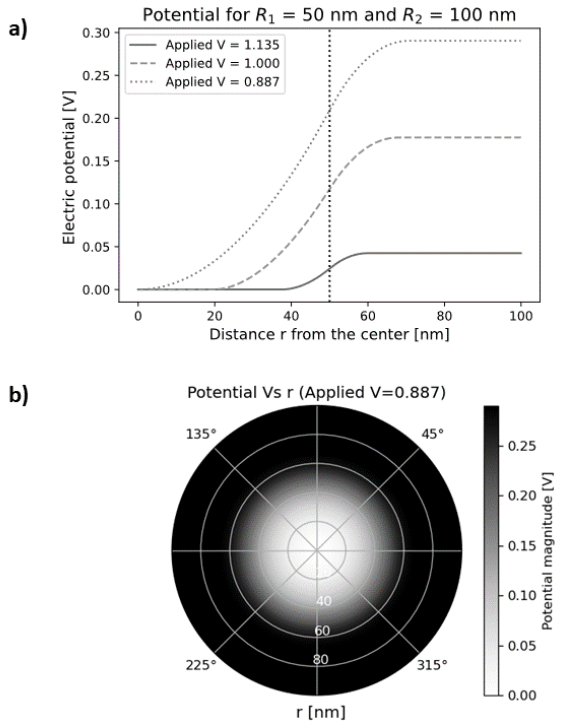

Fig. 12. a) Electric potential in radial terms for the P-N InP homojunction. b) Top view of the potential in the InP P-N homojunction.

V. CONCLUSIONS

A complete electrostatic semi-analytical model for radial nanowire heterojunctions was developed for N-P core-shell semiconductors disposition which can also be used for nanowire homojunction devices. The space charge region extensions in each side can be calculated from the transcendental equations obtained from the solution of the Poisson equation in cylindrical coordinates. In addition, it is possible to determine the electric field and the potential distributions within the nanowire device so that further calculations will be possible for determining the current density vs voltage (J-V) curve of a nanowire solar cell. To illustrate the application of the developed expressions we have shown some examples of heterojunction and homojunction devices. This is the first step to simulate and design high efficiency solar cells based on radial nanowire heterojunctions in the future.

REFERENCES

[1] M. Asif and T. Muneer, "Energy supply, its demand and security issues for developed and emerging economies," Renew. Sustain. Energy Rev., vol. 11, no. 7, pp. 1388–1413, Sep. 2007.

[2] C. Chen et al., "Recent Advances in Solar Energy Full Spectrum Conversion and Utilization," ES Energy Environ., 2021.

[3] A. Schinke-Nendza, F. von Loeper, P. Osinski, P. Schaumann, V. Schmidt, and C. Weber, "Probabilistic forecasting of photovoltaic power supply — A hybrid approach using D-vine copulas to model spatial dependencies," Appl. Energy, vol. 304, p. 117599, Dec. 2021.

[4] A. Ghazy, M. Safdar, M. Lastusaari, H. Savin, and M. Karppinen, "Advances in upconversion enhanced solar cell performance," Sol. Energy Mater. Sol. Cells, vol. 230, p. 111234, Sep. 2021.

[5] E. C. Garnett, B. Ehrler, A. Polman, and E. Alarcon-Llado, "Photonics for Photovoltaics: Advances and Opportunities," ACS Photonics, vol. 8, no. 1, pp. 61–70, Jan. 2020.

[6] J. Zhang, "Solar PV Market Research and Industry Competition Report," IOP Conf. Series: Earth and Environmental Science, vol 632 p. 032047, 2021.

[7] K. T. VanSant, A. C. Tamboli, and E. L. Warren, "III-V-on-Si Tandem Solar Cells," Joule, vol. 5, no. 3, pp. 514–518, Mar. 2021.

[8] Z. Fang et al., "Perovskite-based tandem solar cells," Sci. Bull., vol. 66, no. 6, pp. 621–636, Mar. 2021.

[9] Q. Guo, C.-Y. Wang, T. Hayat, A. Alsaedi, J.-X. Yao, and Z.-A. Tan, "Recent advances in perovskite/organic integrated solar cells," Rare Met. 2021 4010, vol. 40, no. 10, pp. 2763–2777, Feb. 2021.

[10] B. Pal, K. J. Sarkar, and P. Banerji, "Fabrication and studies on Si/InP core-shell nanowire based solar cell using etched Si nanowire arrays," Sol. Energy Mater. Sol. Cells, vol. 204, p. 110217, Jan. 2020.

[11] M. K. Sahoo and P. Kale, "Integration of silicon nanowires in solar cell structure for efficiency enhancement: A review," J. Mater., vol. 5, no. 1, pp. 34–48, Mar. 2019.

[12] K. Korzun, G. W. Castellanos, D. K. G. de Boer, J. G. Rivas, and J. E. M. Haverkort, "Nanowire Solar Cell Above the Radiative Limit," Adv. Opt. Mater., vol. 9, no. 2, p. 2001636, Jan. 2021.

[13] I. Aberg et al., "A GaAs nanowire array solar cell with 15.3% efficiency at 1 sun," IEEE J. Photovoltaics, vol. 6, no. 1, pp. 185–190, Jan. 2016.

[14] L. Hrachowina, Y. Zhang, A. Saxena, G. Siefer, E. Barrigon, and M. T. Borgstrom, "Development and Characterization of a bottom-up InP Nanowire Solar Cell with 16.7% Efficiency," Conf. Rec. IEEE Photovolt. Spec. Conf., vol. 2020-June, pp. 1754–1756, Jun. 2020.

[15] K. Lee et al., "17.6%-Efficient radial junction solar cells using silicon nano/micro hybrid structures," Nanoscale, vol. 8, no. 30, pp. 14473–14479, Jul. 2016.

[16] S. Misra, L. Yu, W. Chen, M. Foldyna, and P. R. i Cabarrocas, "A review on plasma-assisted VLS synthesis of silicon nanowires and radial junction solar cells," J. Phys. D. Appl. Phys., vol. 47, no. 39, p. 393001, Sep. 2014.

[17] E. C. Garnett, M. L. Brongersma, Y. Cui, and M. D. McGehee, "Nanowire Solar Cells," http://dx.doi.org/10.1146/annurev-matsci-062910-100434, vol. 41, pp. 269–295, Jul. 2011.

[18] A. A. Luna, R. B. Correa, J. M. Monsalve, and A. M. Acevedo, "Design of thin film solar cells based on a unified simple analytical model," J. Appl. Res. Technol., vol. 15, no. 6, pp. 599–608, Jul. 2019.

[19] T. Ratz, J.-Y. Raty, G. Brammertz, B. Vermang, and N. D. Nguyen, "Opto-electronic properties and solar cell efficiency modelling of Cu2ZnXS4 (X = Sn, Ge, Si) kesterites," J. Phys. Energy, vol. 3, no. 3, p. 035005, Jun. 2021.

[20] F. A. Abed and L. M. Ali, "Investigation the absorption efficiency of GaAs/InAs nanowire solar cells," J. Lumin., vol. 237, p. 118171, Sep. 2021, doi: 10.1016/J.JLUMIN.2021.118171.

[21] A. C. E. Chia and R. R. LaPierre, "Electrostatic model of radial pn junction nanowires," J. Appl. Phys., vol. 114, no. 7, p. 074317, Aug. 2013.

[22] S. Petrosyan, A. Yesayan and S. Nersesyan, "Theory of nanowire radial p-n-junction" World Academy of Science, Engineering and Technology vol. 71, p. 1065-1070, 2012.

[23] S. K. Agnihotri, D. P. Samajdar, D. V. Prashant, and Z. Arefinia, "Numerical analysis of InP based high efficiency radial junction nanowire solar cell," Opt. Mater. (Amst)., vol. 119, p. 111365, Sep. 2021.

[24] S. M. Sze and K. K. Ng, "Physics of Semiconductor Devices," Phys. Semicond. Devices, Oct. 2006.

[25] M. Yamaguchi, C. Uemura, and A. Yamamoto, "Radiation damage in InP single crystals and solar cells," J. Appl. Phys., vol. 55, no. 6, p. 1429, Jun. 1998.

[26] V. Raj et al., "Indium phosphide based solar cell using ultra-thin ZnO as an electron selective layer," J. Phys. D. Appl. Phys., vol. 51, no. 39, p. 395301, Aug. 2018.